A Novel Approach to the Classification of Regional-Scale Radar Mosaics for Tropical Vegetation Mapping

Matteo Sgrenzaroli, Andrea Baraldi, Gianfranco D. De Grandi, *Fellow, IEEE*, Hugh Eva, and Frédéric Achard

***Abstract*—The Global Rain Forest Mapping (GRFM) radar mosaics, generated from L-band Japanese Earth Resources Satellite 1 imagery downsampled to 100-m pixel size, provide a two-season spatially continuous coverage of the humid tropical ecosystems of the world. This paper presents a novel classification approach suitable for regional-scale vegetation mapping using the GRFM datasets. The mapping system consists of: 1) an application-dependent wavelet-based edge-preserving smoothing algorithm and 2) a two-stage per-pixel hybrid learning nearest multiple-prototype (NMP) classifier, whose unsupervised first stage is a per-pixel near-optimal vector quantizer, called enhanced Linde–Buzo–Gray (ELBG), recently proposed in pattern recognition literature. Identified as ENMP (NMP with ELBG), this novel classification approach is compared against two alternative systems in the classification of forest cover disturbances located across an area in the Amazon Basin. Surface classes of interest are primary forest, degraded forest, nonforest, and water bodies. Reference maps, derived from 30-m resolution Landsat Thematic Mapper imagery, are provided by the National Aeronautics and Space Administration and the Food and Agriculture Organization of the United Nations. Abundant quantitative and qualitative evidence shows that: 1) in a forest/nonforest data-mapping task, ENMP provides a testing accuracy of 87%, in line with training accuracies, i.e., the proposed method seems capable of generalizing well over the GRFM South America dataset and 2) among three competing approaches, ENMP provides the best compromise between ease of use, mapping accuracy, and computational time. Starting from these results, ENMP is employed to generate a swamp forest map of the whole Amazon Basin from the two-season GRFM radar mosaic of South America, in the context of the Global Land Cover project (GLC 2000).**

***Index Terms*—Classification, clustering, radar mosaic, vegetation mapping, wavelet representation.**

I. Introduction

THE GLOBAL Rain Forest Mapping (GRFM) project was initiated by the National Space Development Agency of Japan (NASDA, now JAXA) and conducted by some of the leading Remote Sensing institutions around the world, with the goal of obtaining a two-season spatially continuous radar data coverage of the humid tropical ecosystems of the world [1]–[4]. The entire Amazon Basin, from the Atlantic to the Pacific, was imaged by the Japanese Earth Resources Satellite 1 (JERS-1) L-band synthetic aperture radar (SAR) in September–December 1995, a time corresponding on average to low flooding extent of the Amazon River Basin. The same area, including the northernmost part of South America and Central America, was covered again in May–August 1996, during a high flood period of the Amazon River. The high-resolution (18 m with 12.5-m pixel size) ground range images were processed to compile geocoded and calibrated mosaics at 100-m spatial resolution [2]. The two-season GRFM South America mosaics are referred to as the low-water mosaic and the high-water mosaic, respectively.

Preliminary studies prove that the medium-resolution GRFM radar images are suitable for replacing high-resolution optical images for tropical rain forest extent estimation [5]. In particular, forest maps made from JERS-1 radar images downsampled at 100 m can replace forest maps made from 30-m resolution Landsat TM optical images if: 1) locations where topography dominates the landscape are masked out and 2) radar and optical images are acquired less than one year apart.

Starting from recent developments in the GRFM radar data-mapping systems [6]–[11], this paper presents a novel two-stage data classification scheme (originally proposed in a related conference paper [12]) composed of the following:

- an application-dependent wavelet-based edge preserving smoothing algorithm (a refinement of the method presented in [10]);
- a per-pixel two-stage hybrid learning nearest multiple-prototype (NMP) classifier, whose unsupervised learning first stage consists of the near-optimal enhanced Linde–Buzo–Gray (ELBG) vector quantizer recently proposed in the pattern recognition literature [13]–[15].

This novel classification scheme is hereafter referred to as ENMP (i.e., NMP with ELBG).

In general, it is well known that "if the goal is to obtain good generalization performance in predictive learning, there are no context-independent or usage-independent reasons to favor one learning or classification method over another" [16, p. 454]. In the specific context of the GRFM radar image mapping at continental scale, due to the lack of reference maps with known accuracy and confidence interval, the subjective nature of the GRFM radar data-mapping problem precludes an absolute judgment of competing classifiers. As a consequence, the goal of this paper is to provide enough quantitative and qualitative evidence on the relative efficacy (in terms of mapping accuracy, computation time, and ease of use) of ENMP compared against alter-

Manuscript received May 23, 2003; revised June 6, 2004. This work was carried out in the framework of the Joint Research Center TREES project, which was supported by the DG Environment of the European Commission. The work of M. Sgrenzaroli and A. Baraldi was supported by the European Commission Joint Research Center.

M. Sgrenzaroli is with INN.TEC, 25123 Brescia, Italy.

A. Baraldi is currently Consiglio Nazionale delle Ricerche, CNR-ISSIA, 70126 Bari, Italy.

G. D. De Grandi, H. Eva, and F. Achard are with the European Commission, Joint Research Center, Institute for Environment and Sustainability, 21020 Ispra, Italy (e-mail: frank.de-grandi@jrc.it).

Digital Object Identifier 10.1109/TGRS.2004.836816

TABLE I
RADAR MAPPING APPLICATIONS AT LOCAL AND REGIONAL LEVEL FOR THE LATIN AMERICAN SITE OF THE TREES ERS-1 STUDY 1994 AND THE JERS-1 SCIENCE PROGRAM 1999

Author	Study Area	SAR data set	Set of classes	Classification method	Validation method
Keil M. et al. [27]	Sena Madureira, Acre (Brazil). (2 ERS scene)	ERS-1 SAR C-band, 25 m	Forest / non-forest	* Supervised thresholding for image segmentation. * Segment-based maximum likelihood EBIS classifier.	Comparison with two Landsat TM scenes, field survey along the road, hand-held air photos
Conway J. [28]	Acre (Brazil) (4 ERS scene)	ERS-1 SAR C-band, 100 m	Forest / non -forest	* K-nearest neighbour classifier	Comparison with one Landsat TM scene, NOAA, 1 AVHRR and ATSR-1 scenes.
Corves C. et al. [29]	Manaus region (Brazil)	ERS-1 SAR C-band, 30 m	Forest / non -forest	* Minimum Euclidean distance classifier	Comparison with one Landsat TM scene
Wooding M.G and Batts A. J. [30]	Rondonia (Brazil)	ERS-1 SAR C-band, 25 m, multi-temporal dataset	Forest, scrub/grass, cultivated	* Visual interpretation of multi-temporal colour composites	Comparison with one Landsat TM scene
Grover K. et al.[31]	Tapajos National Park (Brazil)	ERS-1 SAR C-band, 25 m, multi-temporal dataset	Forest (different types), secondary forest, pasture, bare soil	* Speckle noise filtering. * Interactive thresholding for image classification.	Comparison with one Landsat TM scene and SAREX C-band Airborne data
Hoekman D. [32]	Aracuara (Colombia)	ERS-1 SAR C-band, 25 m, multi-temporal dataset	Forest / non-forest, shifting cultivation	* Texture analysis. * Speckle noise filtering. * Wave scattering model.	Comparison with NASA/JPL Airborne SAR (AIRSAR) P-, L- and C-bands
Van der Sanden [33]	Mabura Hill (Guyana)	ERS-1 SAR C-band (PRI and SLC multi-temporal imagery)	Forest (different types), logged forest, non-forest, secondary forest	* Visual interpretation (PRI) * Textural analysis (.SLC).	Field survey
Bijker W. and Hoekman D. [34]	San Jose' del Guaviare (Colombia)	ERS-1 SAR C-band, 25 m, multi-temporal dataset	Forest , non-forest, savannah, pasture	* Speckle noise filtering. * Image segmentation.	Field survey
Dobson et al. [35]	Cabaliana (Brazil)	JERS-1 SAR L-band and ERS-1 SAR C-band combination	Forest (different types), non forest (different classes)	* Edge-preserving speckle noise filtering. * Unsupervised clustering. * Supervised ML cluster aggregation into classes.	Field survey
Dutra L. V. et al. [36]	Acre, Rondonia, Para', Monte Alegre Lake area (Brazil)	JERS-1 SAR L-band, 12.5 m	Deforestation, flooded areas extension	* Texture analysis. * Minimum Mahalanobis distance classifier.	Comparison with Landsat TM scenes, field survey and air photos

native classifiers in a regional-scale mapping pursuit using the GRFM radar dataset.

The rest of the paper is structured as follows. Section II discusses the GRFM dataset classification problem and some related works in tropical forest mapping using synthetic aperture radar (SAR) data. In Section III, study areas, surface classes of interest, and reference data are presented. In Section IV, the wavelet-based edge-preserving smoothing algorithm adopted by ENMP is briefly summarized. In Section V, ENMP is discussed as a classifier potentially suitable for dealing with smoothed GRFM images. Section VI deals with the design of the experimental session. In Section VII, results are compared against those of alternative approaches. In Section VIII, an application of ENMP to regional-scale mapping of tropical forests from the GRFM radar data mosaics is reported. Conclusions are given in Section IX.

II. TROPICAL FOREST MAPPING USING SAR DATA: A REVIEW

Much research work has been recently devoted to the extraction of tropical forest information from radar imagery at either local or global scale. Recently published in remote sensing literature, several Amazon forest-mapping experiments actually deal with single SAR [JERS or European Remote Sensing (ERS)] satellite images, i.e., focus on local-scale mapping. In this category, approaches based on visual inspection [20], [21] or automatic classification [22]–[24] were investigated.

The ERS-1 1994 study [25], within the Tropical Ecosystem Environment observations by Satellites (TREES) project was the first international initiative specifically developed to investigate the relevance and usefulness of spaceborne SAR data for tropical forest mapping at a global scale. In this study, a set of representative forest sites were selected around the tropical belt (eight of them located in South America [26]).

More recently, the GRFM dataset was distributed to the scientific community [1]. To investigate the potential suitability of the TREES and GRFM datasets in tropical forest-mapping tasks, several preliminary studies were conducted on wide-area radar mosaics of ERS-1 and JERS-1 data [27]–[36]. These works are summarized in Table I in terms of study area, type of sensor, spatial resolution, classification scheme (set of classes and classification method), validation method, and reference dataset.

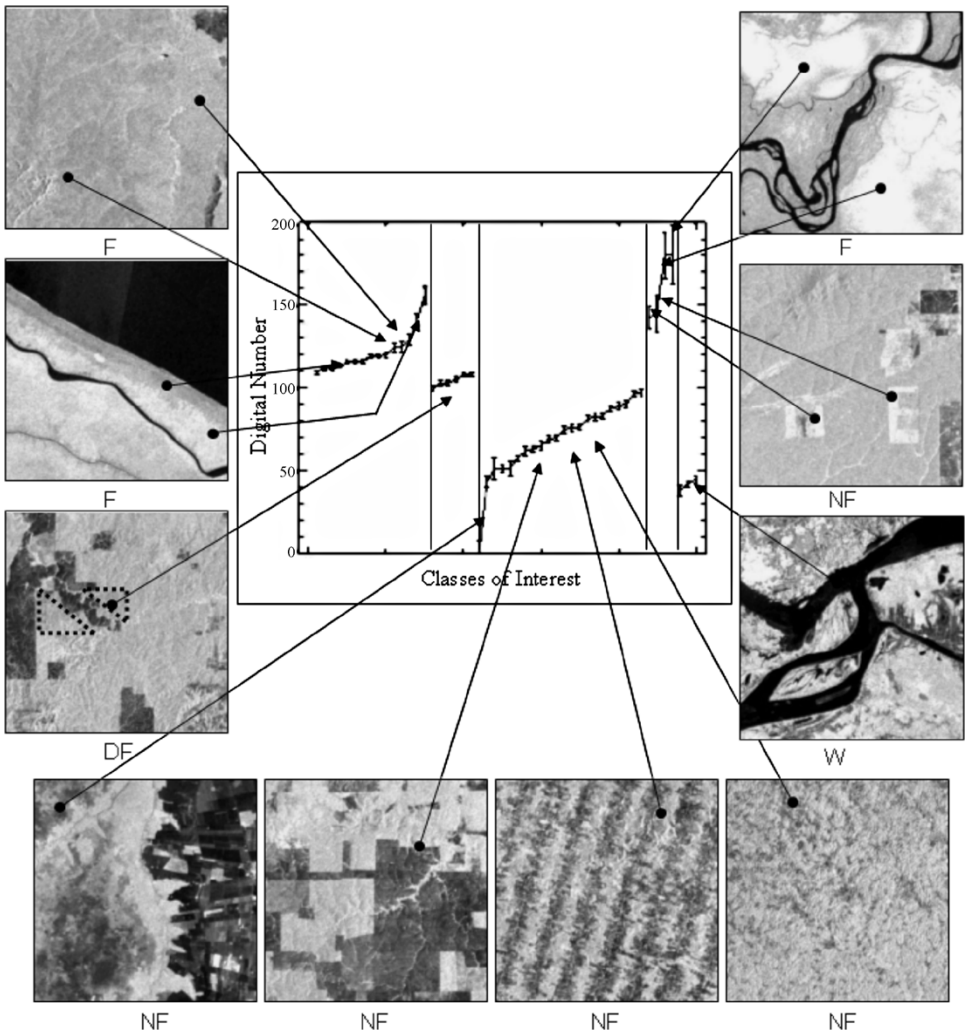

Fig. 1. Synoptic visual description and radiometric characterization of classes *Forest* (F), *Degraded Forest* (DF), *Nonforest* (NF), and *Water* (W).

General issues to be considered when dealing with the GRFM radar datasets are: 1) the size of the datasets that calls for computationally efficient image analysis tools; 2) the presence of multiplicative speckle noise, which suggests the exploitation of a despeckling stage; and 3) the spatial and scaling properties of the surface classes of interest (e.g., forests and urban areas are highly textured), which suggests the use of multiscale data analysis techniques for texture detection.

The last two points indicate that conventional approaches to pattern classification will not work for this kind of dataset. Indeed, clustering techniques that work exclusively in a measurement space while ignoring spatial information (e.g., ISODATA [17]), as well as contextual clustering algorithms (which employ a piecewise constant or slowly varying image model eventually affected by an additive white Gaussian noise field independent of the scene, like the modified Pappas adaptive clustering (MPAC) [18], [19]), are expected to be incapable of dealing with texture (correlation) and/or multiplicative noise, i.e., they are likely to produce oversegmentation.

Instances of bespoke approaches to the classifications of GRFM datasets can be found in [10], [11], and [37].

In [10], two classification strategies, noncontextual (per-pixel) and contextual, respectively, are compared in a one-band GRFM data-mapping problem where three study areas, featuring different patterns of forest cover disturbances, are selected across the Amazon Basin for both training and testing. Classes of interest are forest, nonforest, water, and degraded forest. The noncontextual classification approach, hereafter referred to as NMP with ISODATA (INMP), consists of a per-pixel two-stage hybrid learning NMP classifier [38], whose unsupervised learning first stage adopts an ISODATA clustering algorithm. In the supervised learning second stage of INMP, clusters are gathered into classes of interest according to expert photointerpreters. The second classification approach, hereafter referred to as segment-based NMP (SNMP), is an application-dependent strategy tailored to SAR data. It consists of three modules.

1) An application-dependent wavelet-based edge-preserving smoothing algorithm whose output is a slowly varying approximation of the radar backscatter image plus an edge map where edges are detected as local maxima of the gradient modulus.
2) An application-dependent region growing algorithm, where criteria for detecting initial homogeneous regions and for assigning neighboring pixels in the growth process are based on one-point speckle statistics;

TABLE II
SET OF SURFACE CLASSES (MUTUALLY EXCLUSIVE AND TOTALLY EXHAUSTIVE) AND A SET OF BACKSCATTER PROPERTIES FOR ASSIGNING CLASS LABELS

Surface class	Notes	Surface class components	Average digital number	Backscatter coefficient, σ^0 (dB)
Forest (F)		Dense canopy forest	110	-7.71
		Open canopy	106	-8.03
		Lowland floodplain forest	130	-6.26
		Mangroves forest	105	-8.11
		Flooded forest	255	-0.41
Degraded Forest (DF)	We use the term "degraded forest" to describe any intermediate state from forest to deforestation [10]. Includes disturbed forest areas, partial re-growth, isolated forest patches within non-forest areas, and fragmented forest areas.		105÷130	-6.26÷8.11
Non-forest (NF)	Includes the agricultural land and natural non-forest areas (e.g., cerrado). It cannot be discriminated from partial re-growth (e.g. abandoned pastures).	New clear-cuts	235	-1.11
		Other	100	-8.50
Water (W)	Includes lakes and rivers. Sometimes comparable with bare-soil backscatter.		30	-18.90

3) A segment-based two-stage hybrid learning classifier. In the first stage, the segment mean and standard deviation are computed in the feature extraction step, and a user-defined number of segment categories is reached by clustering segment feature vectors according to a Jeffries–Matusita pairwise minimum-distance criterion. In the supervised learning second stage, unsupervised segment categories are gathered into supervised classes of interest according to expert photointerpreters.

The experimental comparison of INMP and SNMP reveals that, in line with theoretical expectations: 1) noncontextual INMP is faster and easier to use (i.e., it requires fewer user-defined parameters to run) than contextual SNMP and 2) INMP is affected by salt-and-pepper classification noise effects, whereas SNMP pursues a regularization of the mapping solution at the cost of a greater computational load. In synthesis, to improve the tradeoff between ease of use, mapping accuracy, and computational time, conclusions reported in [10] suggest to combine the preprocessing stage of SNMP, providing smooth radar images, with the pixel-based clustering stage of INMP.

III. CLASSES OF INTEREST, STUDY AREAS, AND REFERENCE DATA

The following considerations underpin the design of our classification pursuit.

According to [39], a (crisp) classification scheme is defined by: 1) a set of surface classes that are mutually exclusive and totally exhaustive and 2) a set of rules, or definitions, or properties for assigning class labels. Next, an adequate number of reference samples per class must be gathered, both for training and for the quantitative assessment of mapping results. Indeed, inductive learning problems require a minimum number m_i of independent representative samples per class. Typical rules of thumb require the following.

- $m_i = 5\,D$ (minimum) and $m_i = 100\,D$ (highly desirable if attainable), where D is the data dimensionality [39], [40]. This criterion ensures an adequate estimation of nonsingular/invertible class-specific covariance matrices [40].
- $m_i \geq 30 \div 50$, so that, according to a special case of the central limit theorem, the distribution of many sample statistics becomes approximately normal, which is a basic assumption in several traditional classifiers [41].
- To avoid a poor generalization capability of an induced classifier related to model complexity, the minimum number of per-class representative samples should be $m_{min} \approx W/\varepsilon$, where W is the total number of free parameters, and ε is the classification error. If $\varepsilon = 0.1$, we need around ten times as many training patterns as there are free parameters in the inductive learning system [42].

A. Surface Classes of Interest

In our classification experiment, the definition of the map legend is driven by the need of supporting as a thematic goal the monitoring of two important processes related to land cover change in the tropics: deforestation and forest degradation [45], [46]. Accordingly, surface classes of interest in our classification exercise are: *Forest* (*F*), *Degraded Forest* (*DF*), *Nonforest* (*NF*), and *Water* (*W*). For more details on the rules underpinning these definitions in the forestry domain, the reader is referred to [44] and [45]. A synoptic view of the radiometric characterization of the selected land cover classes is given in Fig. 1 and Table II.

B. Sample Study Areas

In line with the general criteria summarized in the introduction of Section III, a set of four study areas is selected satisfying the following requirements.

- Study sites fall within the so-called "hot spot" deforestation areas defined by the TREES project in the Amazon Basin [43].
- They feature a wide range of biomass and include different land use patterns reflecting the major forms of anthropogenic activities, i.e., they characterize the different patterns of forest cover disturbances occurring within the Amazon Basin.
- In line with [5] (see Section I), for every study site there must be a difference of less than one year between the acquisition dates of the JERS-1 images and the Landsat Thematic Mapper (TM) images used to generate reference maps.

To maintain consistency with experimental results related to classifiers INMP and SNMP, the three study areas used as training sites are the same as those adopted in [10]. Each site of interest covers an area of 185×185 km^2, which is approximately equivalent to the area covered by one Landsat TM image. This corresponds to nine JERS-1 images covering approximately 60×60 km^2 each. Two training areas, located in the Mato Grosso and South Rondonia states of Brazil, are identified as sites 226-69 and 230-69 according to the Landsat TM path-row code. The third training area, located in the Florencia-Napo region in Colombia, is identified as site 8-59. The testing accuracy (measured upon independent testing samples not employed for learning the system's free parameters) is an estimate of the generalization capability of a mapping system. Thus, a fourth study area, located in the North Rondonia state of Brazil and identified with the Landsat TM path-row code 231-68, is adopted as an independent testing site (not included in [10], refer to Section VI-A).

C. Reference Maps

In RS applications, representative samples are typically derived from up-to-date reference data acquired from topographic maps, manually interpreted aerial photographs and/or by ground observations [39]. In our GRFM data-mapping context, thematic maps of the Amazon Basin, generated from Landsat TM images, have been made available, in recent years, by national and international institutions, like the National Aeronautics and Space Administration (NASA) and the Food and Agriculture Organization of the United Nations (FAO). One thematic map, delivered by NASA Tropical Rain Forest Information Center (TRFIC) [44] and derived from a Landsat TM image acquired in 1996 is considered the reference map for the North Rondonia testing site (231-68). In the TRFIC maps, pixel size is 30 m, and the geographic localization error is approximately 500 m.

For training areas 226-69 and 230-69, two TRFIC thematic maps, made from Landsat TM images acquired in 1992 and 1996, respectively, are taken as reference material.

Unfortunately, no TRFIC map is available for the third training site 8-59. In this case, two reference maps at 30-m resolution are derived from Landsat TM data, acquired in 1991 and 1996, respectively, using the hierarchical NMP (HNMP) classifier proposed in [47]. These two maps are validated by means of FAO's forest resource asessment maps. The FAO maps, generated by visual interpretation of Landsat TM scenes acquired in 1990 and 1996, respectively, feature a minimum mapping unit of 100 ha.

Classes in the reference TRFIC maps are designated as: 1. Forest, 2. Deforested areas, 3. Forest regrowth, 4. Water, 5. Cloud, 6. Cloud Shadow, and 7. Cerrado. For comparison with classes *F*, *DF*, *F*, and *W* extracted from the GRFM radar dataset, the original TRFIC classes are combined into metaclasses according to Table III.

Comparison of the high-resolution TRFIC and HNMP reference maps (derived from Landsat TM data) with medium-resolution maps, generated from the GRFM radar data, is made possible by: 1) downsampling reference maps from 30 to 100 m, to make the spatial resolution of reference and radar maps the same and 2) coregistering reference maps with radar maps by means of tie-points selected by visual inspection.

TABLE III
RELATIONSHIP BETWEEN CLASSES DEFINED IN THE TRFIC THEMATIC MAPS AND THE GRFM RADAR MAPS

TRFIC Thematic Classes	Thematic Metaclasses
5. Cloud	0. Unclassified
6. Cloud Shadow	
4. Water	1. Water (W)
1. Forest	2. Forest (F)
3. Re-growing Forest	3. Degraded forest (DF)
2. Deforested 7. Cerrado	4. Non-forest (NF)

The complete set of reference maps employed for result assessment and validation is summarized in Table IV. It has to be noted that quantitative accuracy figures and confidence intervals for the reference maps are not available. As a consequence, an absolute judgment of competing systems is precluded, which is tantamount to saying that, unfortunately, no target accuracy can be specified for the mapping exercise described here. However, at the time this work was performed, the adopted reference maps were considered by the scientific community working on tropical vegetation monitoring as the best spatially explicit reference material available at regional scale. As such, they constitute the only practical if not optimal choice for a map validation exercise at the regional scale.

IV. WAVELET-BASED MULTISCALE EDGE-PRESERVING SMOOTHING

Wavelets have been applied to radar image analysis and processing in recent years [48]–[57]. De Grandi *et al.* [57] have proposed a wavelet-based edge-preserving smoothing algorithm for SAR images. The algorithm is based on a dyadic wavelet that works as a differential operator [58] and a multiscale edge detection approach proposed in [59] and [60]. An improved version of this algorithm is at the core of the preprocessing step of ENMP. Other applications of the same approach can be found in [55] and [56]. Statistical characterization and performance analysis of the algorithm with special emphasis on the case of multiplicative speckle noise are being considered for publication in a specific paper. The main components of the smoothing algorithm can be summarized as follows (see block diagram in Fig. 2).

1) *Image model.* The radar image model takes into account how the radar backscatter changes with scale for: 1) homogeneous areas featuring stationary texture and speckle statistics and 2) nonstationary image structures like image step edges, lines, and point targets.
2) *Wavelet modulus maxima tracking*. Tracking positions and values of the wavelet modulus maxima through spatial scales is the fundamental mechanism underpinning the edge-preserving smoothing algorithm by image synthesis (reconstruction).
3) *Wavelet thresholding for denoising and texture smoothing.* An application-specific rule-based mechanism is applied to distinguish between gradient modulus

TABLE IV
SUMMARY OF THEMATIC MAPS DERIVED FROM LANDSAT TM AND JERS-1 IMAGERY, USED FOR RESULT ASSESSMENT AND VALIDATION (* ACQUISITION DATE NOT AVAILABLE)

SITE (Landsat TM path-row)	**RADAR MAPS**			**REFERENCE MAPS**
	INMP	**SNMP**	**ENMP**	
226-69 Mato Grosso (training)	NASDA JERS-1 Level 2.1 (100 m) 15 Nov. 92	NASDA JERS-1 Level 2.1 (100 m) 15 Nov. 92	–	TRFIC TM 19 May 92
	–	–	GRFM mosaic Sept.-Dec. 95	TRFIC TM 31 July 96
230-69 South Rondonia (training)	NASDA JERS-1 Level 2.1 (100 m) 5 April 93	NASDA JERS-1 Level 2.1 (100 m) 5 April 93	–	TRFIC TM 15 May 92
	–	–	GRFM mosaic Sept.-Dec. 95	TRFIC TM 13 July 96
8-59 Florencia Napo (training)	NASDA JERS-1 Level 2.1 (100 m) 14 Nov. 92	NASDA JERS-1 Level 2.1 (100 m) 14 Nov. 92	–	HNMP TM 2 March 91
	–	–	GRFM mosaic Sept.-Dec. 95	HNMP TM 11 Aug. 96
231-68 North Rondonia (testing)	–	–	GRFM mosaic Sept.-Dec. 95	TRFIC TM 1996*

local maxima related to forest/nonforest interclass transitions (to be preserved), from those related to forest within-class texture variations (to be removed).

4) Reconstruction from regularized neighborhoods of selected wavelet modulus maxima. Scope of this step is to reconstruct an edge-preserving smoothed signal by moving from coarser to finer resolution. The reconstruction is achieved by means of an inverse wavelet transform while exploiting the evolution with scale of wavelet modulus local maxima detected by the tracking algorithm.

V. CLASSIFICATION METHOD

Section II pointed out that robust mapping using radar data may realistically stem from systems exploiting multiscale image analysis criteria. Hereafter, a novel GRFM data-mapping scheme, ENMP, is proposed as a synthesis between the INMP classifier, which is noncontextual (pixel-based) and computationally efficient, and the SNMP classifier, which is contextual but computationally expensive (as pointed out in a related paper [10]). In deeper detail, to combine high classification accuracy with low processing time, a computationally efficient per-pixel (i.e., noncontextual) clustering algorithm, similar to that adopted in INMP, is fed with a smoothed approximation of the radar data at full resolution similar to that computed by the SNMP preprocessing block.

Main building blocks of ENMP are shown in Fig. 3. In line with [11], it is the preprocessing stage of ENMP (block 1) that takes multiscale contextual information into account by implementing the wavelet decomposition and reconstruction algo-

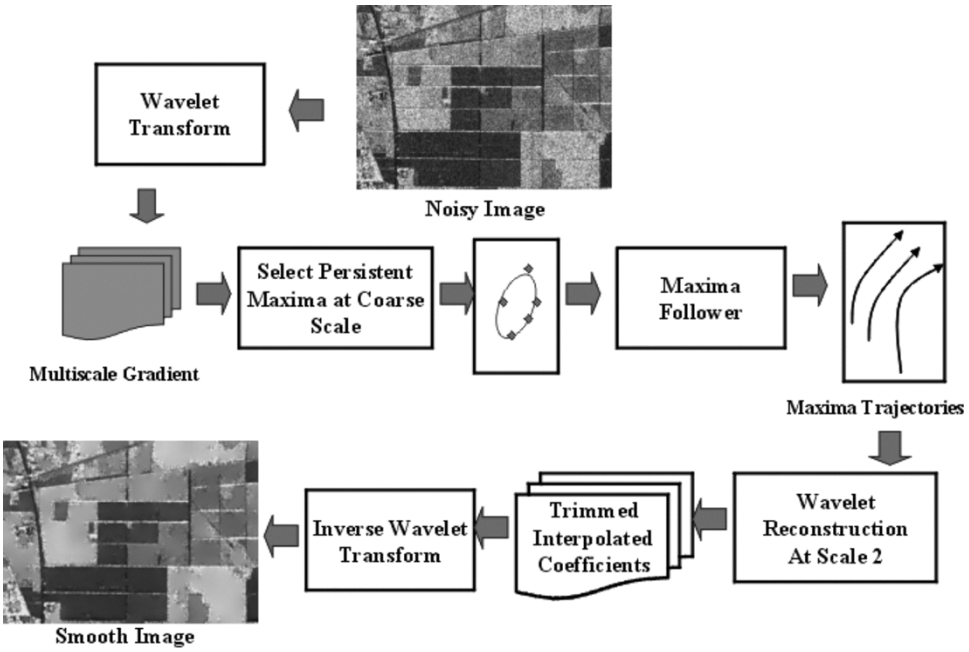

Fig. 2. Block diagram of the wavelet-based algorithm for the generation of edge-preserving piecewise smooth approximations of the radar imagery.

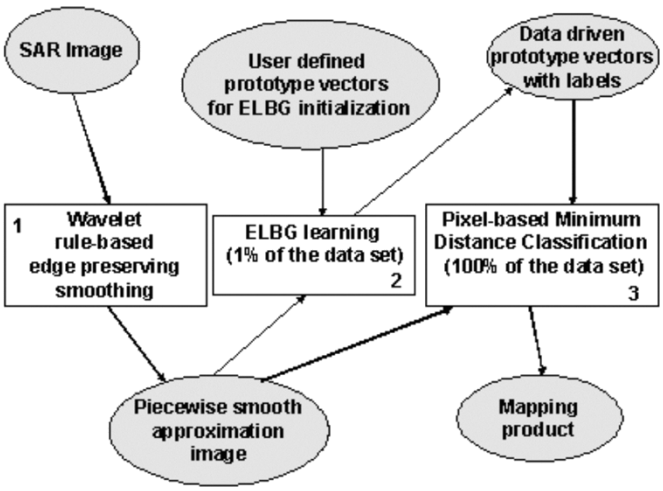

Fig. 3. Building blocks of ENMP. Computational processes are in rectangles, datasets in ovals.

rithm summarized in Section IV. Block 2 of ENMP consists of a per-pixel two-stage hybrid learning classifier whose unsupervised learning module is implemented by the ELBG vector quantization algorithm. This algorithm was recently proposed in pattern recognition literature as an improvement over the well-known LBG (i.e., hard c-means) vector quantization algorithm [13]–[15]. It is a batch learning nonconstructive vector quantizer, i.e., it tries to minimize a distortion error, or mean square error (MSE), with a fixed number of codewords that must be user-defined. The original contribution of ELBG is to employ local optimization criteria, which may require codewords to move across noncontiguous Voronoi regions, to reduce the global distortion (quantization) error. This makes ELBG nearly optimal and stable, i.e., its output results are virtually independent of the initial position of templates. At the second stage of the hybrid learning classifier, template vectors are labeled. In general, many-to-one relationships between unsupervised template vectors (codewords) and land cover classes of interest can be defined by an expert photointerpreter or by supervised learning techniques [42]. In block 3, each pixel is labeled according to the minimum-distance-to-prototype criterion.

It is noteworthy that, to improve the noncontextual ELBG clustering step without requiring additional supervision, ELBG may be followed in cascade by the context-sensitive multiscale modified Pappas adaptive clustering (MPAC) algorithm [18]. MPAC is capable of detecting genuine, but small, image details at the cost of an additional computational overhead. Since the suboptimal MPAC block is in cascade with ELBG, the performance of the former largely depends on the quality of the initialization provided by the latter. In any event, exploitation of MPAC was not pursued further in the present work for computational reasons.

VI. Experimental Session Design

The proposed ENMP classification approach is compared against the INMP and SNMP classifiers using the low-water backscatter GRFM South America radar mosaic, where four independent study areas are located. These sites feature different forest cover disturbances and are documented by reference maps (refer to Section III). This choice allows for compatibility with the experiments comparing SNMP with INMP reported in [10].

A. Reference Data Resampling Strategy

In practice, any representative data resampling method for mapping accuracy assessment does the following.

1) Resamples reference data into training and testing datasets. On the one hand, if the training set is small, then the induced classifier will not be robust (to changes in the training set) and will have a low generalization capability. On the other hand, when the test set is small, then the confidence in the estimated error rate will be low [17].

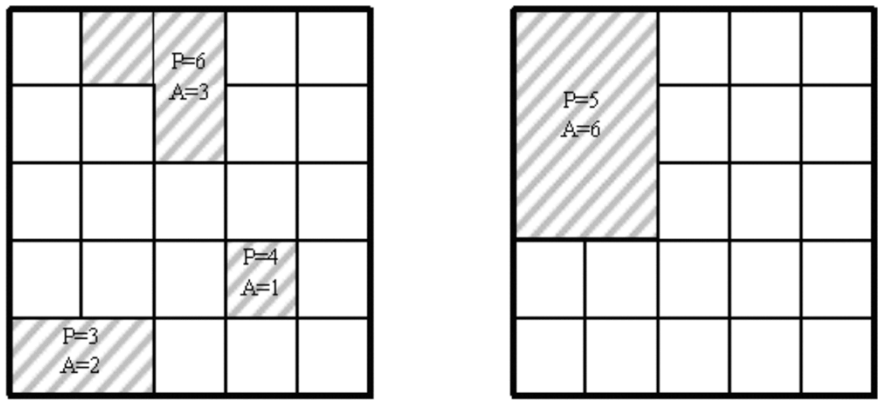

$$PA = \frac{1}{m}\cdot\sum_{k=1}^{m}\frac{P_k}{A_k} = \frac{1}{3}\left(\frac{6}{3}+\frac{3}{2}+\frac{4}{1}\right) = 2.5 \qquad PA = \frac{5}{6} = 0.83$$

Fig. 4. Examples of perimeter-over-area ratio (PA) computations.

2) Takes the empirical testing error as an estimate of the true error rate [4], [5], [7]. Typical error estimation methods for induced classifiers are the holdout, leave-one-out, n-fold cross validation, and the bootstrap method (for a detailed discussion, refer to [7], [16], and [18]).

In our case, to maintain consistency with results in [10], reference data, provided by four study areas, are resampled into training and testing datasets according to an holdout validation method (where a typical reference data partition is 2/3 for training and 1/3 for testing [62]). In particular, in line with [10], three study areas (226-69, 230-69, and 8-59) are adopted as training sites (i.e., to generate induced classifiers), and one study area (231-68) as testing site to assess the generalization capability of competing classifiers (not considered in [10]). It is noteworthy that training samples collected from training sites (226-69, 230-69, and 8-59) account for only 1% of the whole dataset, i.e., the classification problem at hand is likely to be poorly to ill-posed [61].

B. Implementation Parameters

The ELBG clustering stage of ENMP is run on the training dataset (consisting of training sites 226-69, 230-69, and 8-59) with a number of prototypes (also called clusters or template vectors) equal to 16. The user-defined number of cluster prototypes is set arbitrarily larger than four, which is the number of surface classes (as required by NMP classifiers [38]), but sufficiently small to be feasible for expert photointerpreters to detect many-clusters to one-class relationships at the second stage of ENMP. The number of maximum iterations is set to 10, which is sufficient for ELBG to reach convergence.

To be consistent with ELBG, the ISODATA clustering stage of INMP, implemented by the ENVI image processing software toolbox (ENVI is a product of RSI, Inc. [63]), employs 16 clusters, and a per-class label change default value of 2% to reach termination.

In SNMP, the number $M_{\max}$ of pixels required to gather robust segment-based statistics is set to 49, and the theoretical variance of a homogeneous region is computed according to the procedure outlined in [3]. In the region-merging step, the final number of segment-based categories is set equal to 16, to be consistent with the final number of clusters detected by ENMP and INMP. Owing to their preprocessing filtering stage, SNMP and ENMP are more difficult to use (i.e., have more free parameters, which are less intuitive to set) than INMP, while ENMP is easier to use than SNMP.

C. Map Quality Measures

Quantitative assessment of the fidelity of the map to reference data implies evaluating: 1) the labeling (i.e., thematic) fidelity of the map to reference data [64] and 2) the spatial distribution of classification errors [65].

1) Labeling Fidelity of the Map to Reference Data: The labeling fidelity of the map to reference data, also known as *thematic accuracy* [39], is typically investigated by a confusion matrix (error matrix) [66]. The confusion matrix is currently at the core of land cover classification accuracy assessment literature because it provides an excellent summary of the two types of thematic errors that may occur, namely, omission and commission errors [65].

In line with [67], confusion matrices between radar and reference maps are computed in this paper. In order to shrink the confidence interval (i.e., variance) of a classification accuracy estimate, the number of testing samples must be sufficiently large (see Section VI-A). Therefore, each confusion matrix is generated from 300 class-specific samples randomly selected from the study site at hand (consistently with the criteria listed in Section III).

There are many well-known measures of accuracy that can be derived from a confusion matrix, e.g., overall accuracy (OA), normalized accuracy, producer's accuracy, user's accuracy, Kappa coefficient ($\hat{K} \in [-1, 1]$), variance of $\hat{K}$, Z coefficient, etc. [39]. In general, OA (defined as the sum of the confusion matrix diagonal elements), normalized accuracy, and coefficient $\hat{K}$ (which exploits all matrix elements) tend to disagree [39], thus reflecting different information contained in the error matrix. In line with the comparison between SNMP and INMP proposed in [10], coefficient $\hat{K}$, which is the standard

TABLE V
COMPARISON OF CLASSIFIERS INMP, SNMP, AND ENMP FOR TRAINING SITES 226-69, 230-69, AND 8-59. REFERENCE MATERIAL CONSISTS OF TRFIC MAPS (SITES 226-69 AND 230-69) AND MAPS DERIVED FROM LANDSAT TM IMAGES USING THE HNMP CLASSIFIER (SITE 8-59)

Site	Classification method	$\hat{K}$	$\mathrm{var}(\hat{K})$	$\tilde{K}$	Z
226-69	INMP	0.603	0.000482	27.47	
	SNMP	0.605	0.000457	28.30	$0.06_{\lvert SNMP - INMP \rvert}$
	ENMP	0.758	0.000230	49.98	$5.83_{\lvert ENMP - SNMP \rvert}$
230-69	INMP	0.265	0.000681	10.18	
	SNMP	0.407	0.000557	17.24	$4.03_{\lvert SNMP - INMP \rvert}$
	ENMP	0.621	0.000342	33.57	$7.13_{\lvert ENMP - SNMP \rvert}$
8-59	INMP	0.205	0.000967	6.61	
	SNMP	0.303	0.000780	10.86	$2.34_{\lvert SNMP - INMP \rvert}$
	ENMP	0.579	0.000543	24.84	$7.58_{\lvert ENMP - SNMP \rvert}$

TABLE VI
OVERALL ACCURACY (OA) VALUES RELATED TO CLASSIFIERS INMP, SNMP, AND ENMP FOR TRAINING AREAS 226-69, 230-69, AND 8-59. THE CLASSIFICATION DISCREPANCY BETWEEN REFERENCE MAPS AND MAPS DERIVED FORM RADAR DATA INCREASES WITH THE PA RATIO OF DEFORESTATION PATTERNS CALCULATED FOR CLASS F IN REFERENCE MAPS

Training Site	OA INMP	OA SNMP	OA ENMP	PA (class forest in reference map)
226-69	86%	91%	92%	0.057
230-69	66%	73%	84%	0.144
8-59	55%	57%	82%	1.037

component of most classification accuracy assessments [68], is adopted in this paper. Concerns related to the definition and different ways of computing chance agreement P(E), a fundamental component of the Kappa statistic, have been reported in the literature [71]. The main condition underpinning the validity of P(E) is the statistical independence of the raters. This condition is satisfied in our case, where the raters are two different classification procedures using different datasets.

The range of $\hat{K}$ is qualitatively ranked as strong agreement $\hat{K} > 0.8$, moderate agreement $0.4 < \hat{K} < 0.8$, and poor agreement $\hat{K} < 0.4$ [68]. Let $\hat{\mathrm{var}}(\hat{K})$ be the estimates of the variance of $\hat{K}$ [69]. The test statistic for testing the significance of a single error matrix becomes

$$\tilde{K} = \frac{\hat{K}}{\sqrt{\hat{\mathrm{var}}(\hat{K})}}. \tag{1}$$

For example, if $\hat{K} > 1.96$, then the classification is significantly better than a random classification at the 95% confidence level [39]. To test whether two independent error matrices are significantly different in statistical terms, the following relation is adopted [69]:

$$Z_{|A-B|} = \frac{|\hat{K}_A - \hat{K}_B|}{\sqrt{\hat{\mathrm{var}}(\hat{K}_A) + \hat{\mathrm{var}}(\hat{K}_B)}} \tag{2}$$

where $Z_{|A-B|}$ is standardized and normally distributed. Thus, if $Z_{|A-B|} < 1.96$, then $\hat{K}_A$ and $\hat{K}_B$ are significantly different at the 95% confidence level [39].

2) Spatial Distribution of Classification Errors: The spatial distribution of classification errors, also known as *location accuracy* [39], is a major concern in most RS image-mapping projects [65]. Nonetheless, because accuracy metrics derived from the traditional confusion matrix provide no information on the spatial distribution of classification errors, then the estimation of the spatial fidelity of maps to reference data is ignored in practice in RS literature [39]. A possible solution is to replace the difficult problem of locational accuracy assessment with the more tractable problem of assessing the spatial fidelity of maps to reference data, irrespective of their labeling [19]. This is equivalent to comparing maps with a reference partition in terms of segmentation quality indexes, which is a well-known problem in image processing [19], [66].

In the context of RS image-mapping problems, a segmentation quality index can be computed if: 1) the reference sample data form a two-dimensional lattice (image), termed *reference map* or *ground truth image* [70] and 2) a segmentation process partitions the map (under investigation) as well as the ground truth image into segmented images, where each *segment* (also called *region*) is made of connected pixels belonging to the same (supervised) class (in case of a classification map) or (unsupervised) category type (in case of a cluster map) and is provided with a unique (segment-based) identifier.

A variety of measurements can be performed to numerically describe spatial patterns (landscape fragmentation). In our analysis, the average perimeter-over-area (PA) ratio is adopted as a typical measure of shape complexity [39], [72], [73]

$$\begin{aligned} \mathrm{PA} &= \frac{1}{m} \cdot \sum_{k=1}^{m} \frac{P_k}{A_k} \\ m &= \text{total numer of segments} \\ P_k &= \text{perimeter of the } k\text{th segment} \\ A_k &= \text{area of the } k\text{th segment.} \end{aligned} \tag{3}$$

TABLE VII
TRAINING OVERALL ACCURACY (OA) USING ENMP FOR TRAINING SITES MATO-GROSSO (226-69), SOUTH RONDONIA (230-69), AND FLORENCIA-NAPO (8-59) COMPARED WITH THE TESTING OA FOR THE NORTH RONDONIA (231-68) TEST SITE

Classes	Training OA			Testing OA
	230-69	226-69	8-59	231-68
A	83%	72%	58%	77%
B	86%	75%		
C	92%	84%	82%	87%

A: classes W, F, DF, NF
B: classes W, F, DF, NF excluding cerrado
C: classes F, NF

230-69 Mato Grosso
226-69 South Rondonia
8-59 Florencia-Napo
231-68 North Rondonia

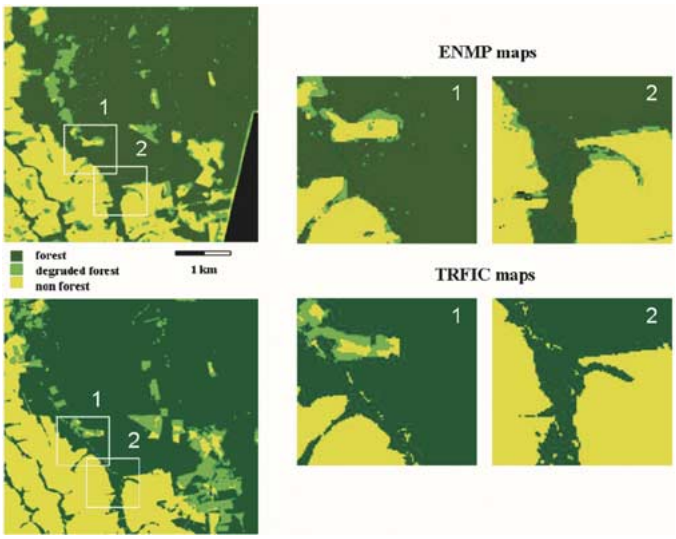

Fig. 5. Visual comparison between the ENMP map and the TRFIC reference map. Mato Grosso training site (226-69), where deforestation is mainly due to ranching and selective logging.

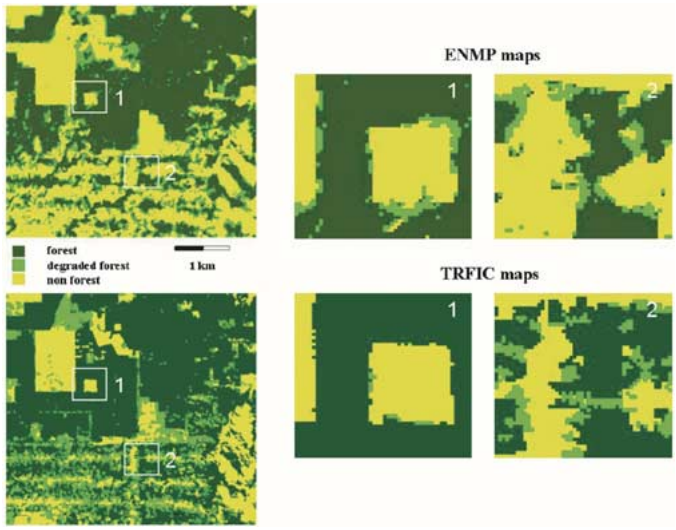

Fig. 6. Visual comparison between the ENMP map and the TRFIC reference map. South Rondonia training site (230-69), characterized by massive deforestation following linear patterns.

In our experiments, perimeter values are computed as four-adjacency neighbors where pixel locations outside of the image boundary are ignored (see some PA ratio computation examples in Fig. 4). In this case, $0 < \mathrm{PA} \leq 4$. In general, when class labels tend to gather in compact large segments, PA values tend to stay low (i.e., tend to 0), while fragmented maps feature larger PA values (i.e., tend to 4). In other words, the PA measure increases when the separability between label types (which can be related to pure substances or fluids) decreases, i.e., when the common boundary between different label types increases.

VII. RESULT ASSESSMENT

Discrepancies between radar and reference maps may be caused by the following phenomena:

1) real vegetation changes between JERS-1 and Landsat TM data acquisition dates (those changes could have a natural (phenology) or an anthropic cause);
2) differences between imaging systems, wave scattering mechanisms, and classification approaches;
3) coregistration problems.

Owing to these effects, large discrepancies between radar maps and reference optical maps are expected to occur across the boundary between cerrado (belonging to class *NF*, see Section III-A) and the humid forest ecosystem because of the sensitivity of radar signal to: 1) forest biomass in transition areas (whereas the optical signal is related to the canopy reflectance); 2) topographic effects; and 3) soil moisture conditions (relevant when the radar signal propagates through a low density canopy).

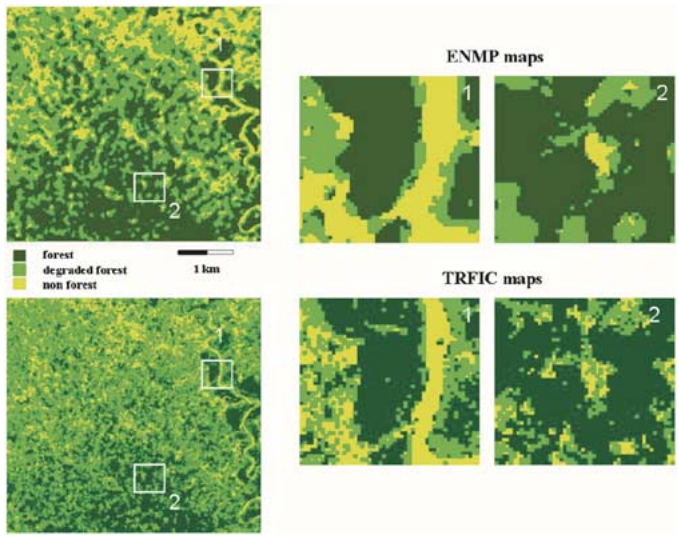

Fig. 7. Visual comparison between the ENMP map and the HNMP reference map. Florencia-Napo training site (8-59), featuring deforestation with linear and diffuse patterns.

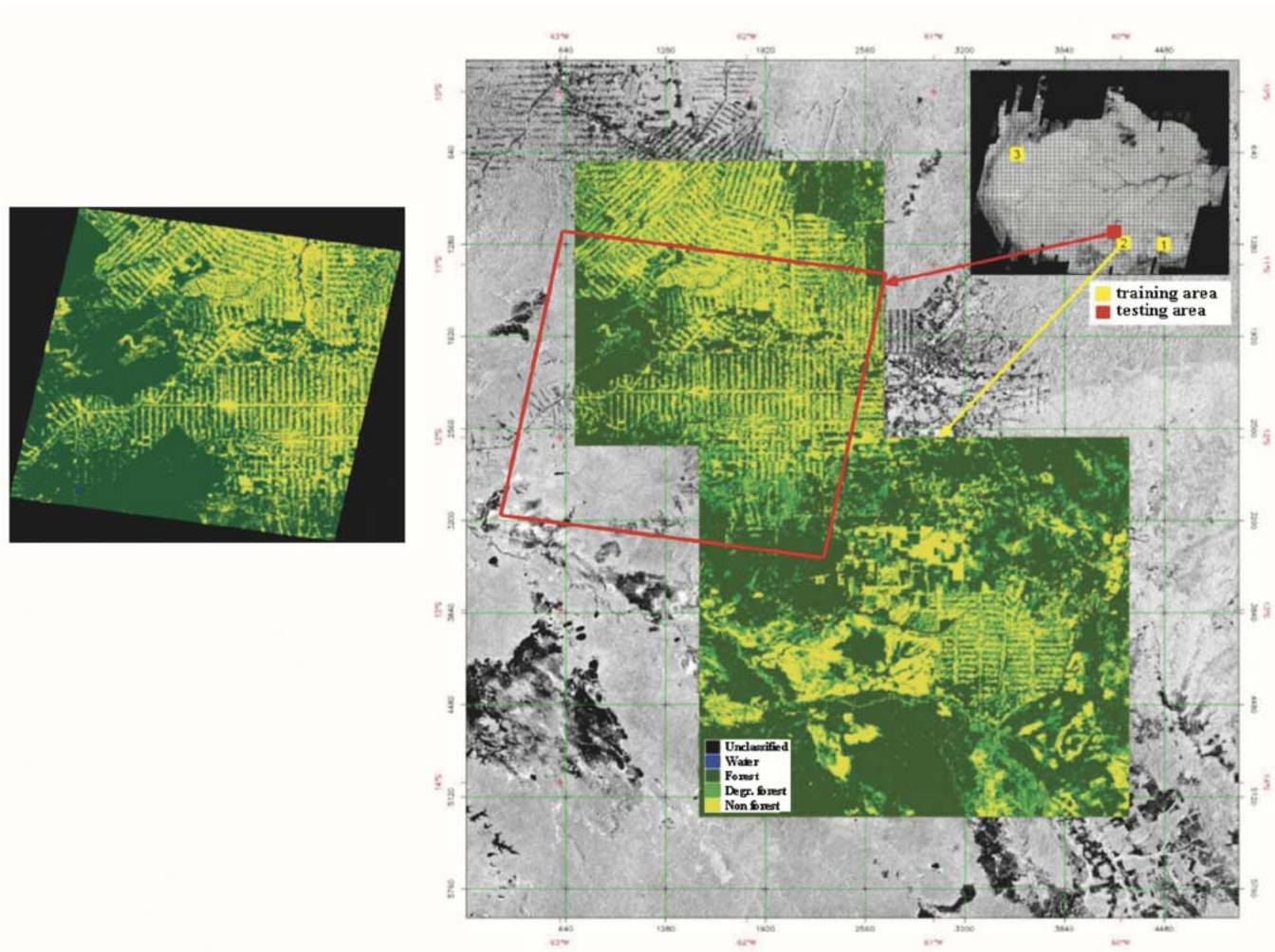

Fig. 8. ENMP maps of the North Rondonia testing site (231-68) and the South Rondonia training site (230-69). The TRFIC map which overlaps the testing site is shown on the left. The whole GRFM South America mosaic is shown in the inset at the upper right corner.

A. *Quantitative Assessment of Results*

In [10], a detailed analysis of the labeling performances of INMP and SNMP over training sites 226-69, 230-69, and 8-59 can be found. As summarized in Table V (adapted from [10]), confusion matrix quality measures of INMP, SNMP, and ENMP collected over training areas 226-69, 230-69, and 8-59 indicate that ENMP features superior accuracy ($\hat{K}$), greatest difference from random classification ($\hat{K} > 1.96$, at the 95% confidence level) and strongest difference with respect to error matrices of other classifiers ($Z > 1.96$, at the 95% confidence level).

Table VI highlights the relationship between OA values for classes *F* and *NF* over the three training areas and the PA ratio relative to spatial patterns of class *F* extracted from the reference map (refer to Table IV for details about reference data). In line with Table V, these results confirm that in terms of training OA values, ENMP outperforms SNMP, which is in turn superior to INMP. Moreover, Table VI shows that ENMP is more robust (less sensitive) than SNMP and INMP to changes in the fragmentation of class *F*. In other words, ENMP seems more capable than SNMP and INMP of detecting genuine but small image details. Finally, Table VI shows that in line with theoretical expectations, the classification discrepancy between reference and radar maps increases with the PA ratio (i.e., with the fragmentation) of class *F* in reference maps for all competing classifiers. This may be due to the following:

1) differences in spatial sampling between the 100-m resolution GRFM dataset and the 30-m resolution Landsat TM reference data;
2) coregistration errors that increase where the landscape complexity is higher;
3) higher dynamics of surface changes in highly fragmented zones between two acquisition dates (e.g., due to anthropogenic activities);
4) inability of the radar classification algorithm to detect genuine but small regions of interest.

The generalization capability of ENMP is investigated in Table VII, comparing the OA values of ENMP over the training sites of Mato-Grosso (226-69), South Rondonia (230-69), and Florencia-Napo (8-59) against the OA value over the testing site of North Rondonia (231-68). In Table VII and row B, instances of training site 8-59 (Florencia-Napo) and the testing site (North Rondonia) are empty because class *cerrado* is not present in these sites. Table VII shows that when class set A (consisting of classes *W*, *F*, *DF*, and *NF*) is involved, the testing accuracy, equal to 77%, is in line with training accuracies. The major source of misclassification is identified

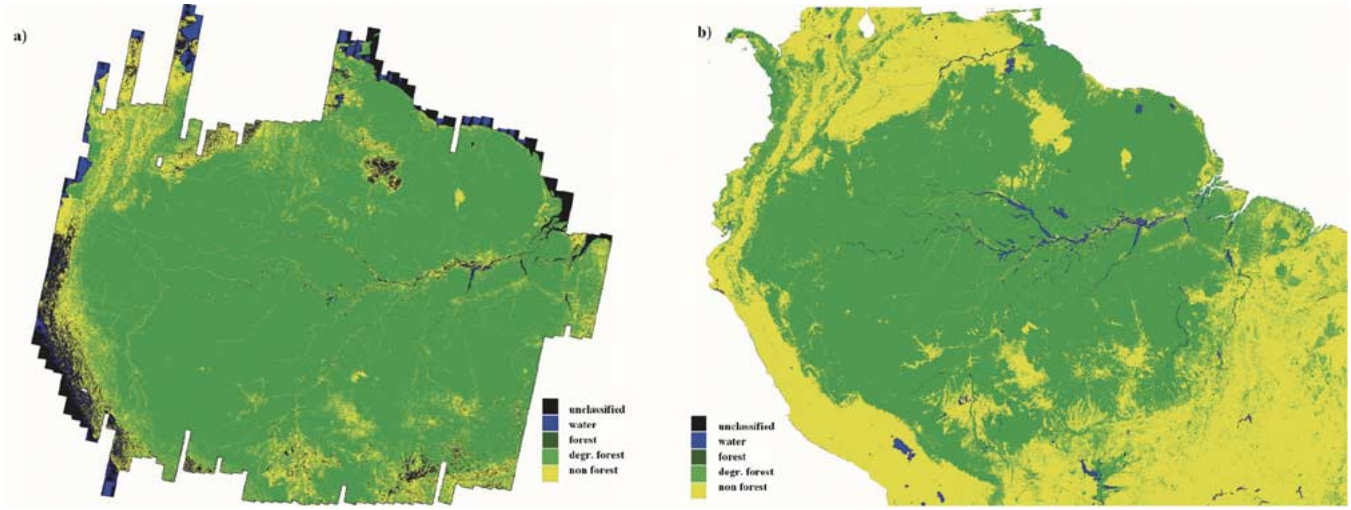

Fig. 9. ENMP map of the low-water season GRFM South America mosaic (a) downsampled from 100 m to 1.2 km. ERS ATSR-2 TREES vegetation map (b) at 1.2-km spatial resolution. To match the legends of the two maps, classes *evergreen forest, dry forest, and mangroves* in the TREES map are color-coded as class *forest* (F) in the ENMP map, *open/fragmented forest* as class *degraded forest* (DF), *plantation, nonforest, and semievergreen forest/shrubs* as class *nonforest* (NF).

TABLE VIII
BENCHMARK OF INMP, SNMP AND ENMP CLASSIFIERS WITH RESPECT TO PROCESSING TIME

	INMP	**SNMP**	**ENMP**
Total time (min)	1	20	8
Wavelet reconstruction	NA	5	5

in class *DF*. When this class is removed from classification, the testing accuracy increases to 87%. This forest/nonforest testing value is superior to the U.S. Geological Survey classification accuracy requirement (equal to 85%). Above all, the testing accuracy is comfortably close to training accuracies (which are optimistically biased). In other words, this value seems realistic and capable of accounting for the unknown quality of reference maps (also affected by spatial downsampling; refer to Section III-C).

The experimental results shown in Table VII are also consistent with theoretical expectations. On the one hand, the discrepancy between radar and reference optical maps increases when considering the boundary regions between *cerrado* (belonging to class *NF*; refer to rows A and B of Table VII) and the low backscattering surface belonging to class *DF* (due to clearing or regrowth). On the other hand, high backscattering values of class *DF* (due to stems that were recently felled and lie on the ground) may overlap with those of flooded forest (which belong to class *F*).

The ENMP maps relative to training sites 226-69, 230-69, and 8-59 are visually compared with reference maps in Figs. 5–7, respectively. In Fig. 8, the ENMP maps over the North and South Rondonia sites (231-68 and 230-69) are combined to be visually compared with the TRFIC map that partially overlaps with the testing area.

B. Qualitative Assessment of Generalization Capabilities

To qualitatively (visually) assess the generalization capability of the ENMP classifier on the entire low-water season GRFM South America radar mosaic, the following procedure is set up. First, the GRFM mosaic is downscaled from 100- to 1200-m pixel size. Due to the large number of equivalent looks, this dataset does not need to be preprocessed for speckle removal. Next, ELBG is run with 32 prototype vectors on the entire dataset. Finally, clusters are combined into classes of interest *F*, *DF*, *NF*, and *W* as shown in Fig. 9(a). According to expert photointerpreters, this classification map at 1.2-km resolution is qualitatively consistent with the JRC-ESA TREES project forest map [43]. This map [see Fig. 9(b)] was derived from 300 ERS ATSR-2 optical images acquired between 1998 and 2000. Thematic classes are: *water, evergreen forest, dry forest, mangrove, open/fragmented forest, plantation, nonforest, and semievergreen forest/shrubs ("Chaco")*. In Fig. 9(b), classes *evergreen forest, dry forest, mangroves* are color-coded as class *F*, *open/fragmented forest* as class *DF*, *plantation, nonforest, and semievergreen forest/shrubs* as class *NF*.

C. Computational Performance Assessment

In terms of computational time, classifiers INMP, SNMP, and ENMP are compared on a training dataset equivalent to a GRFM data block of 660×660 pixels in size. The clustering stage of the three classifiers detects a final number of clusters equal to 10. The number of clustering iterations of classifiers INMP and ENMP is set to 10. Processing times are shown in Table VIII when all classifiers are run on a Sun Microsystems SPARC II 400-MHz workstation. This table reveals that the improved accuracy of SNMP with respect to INMP is achieved at the cost of an increased computational time that may become soon unacceptable in mapping tasks at the regional scale.

VIII. FURTHER DEVELOPMENTS

According to our training and testing results, based on both qualitative and quantitative map quality assessments (see Section VII), ENMP seems to provide a clear improvement in the tradeoff between classification performance, computational time, and ease of use (i.e., user-defined parameters, if any, are easier to select) with respect to other classification approaches like INMP and SNMP.

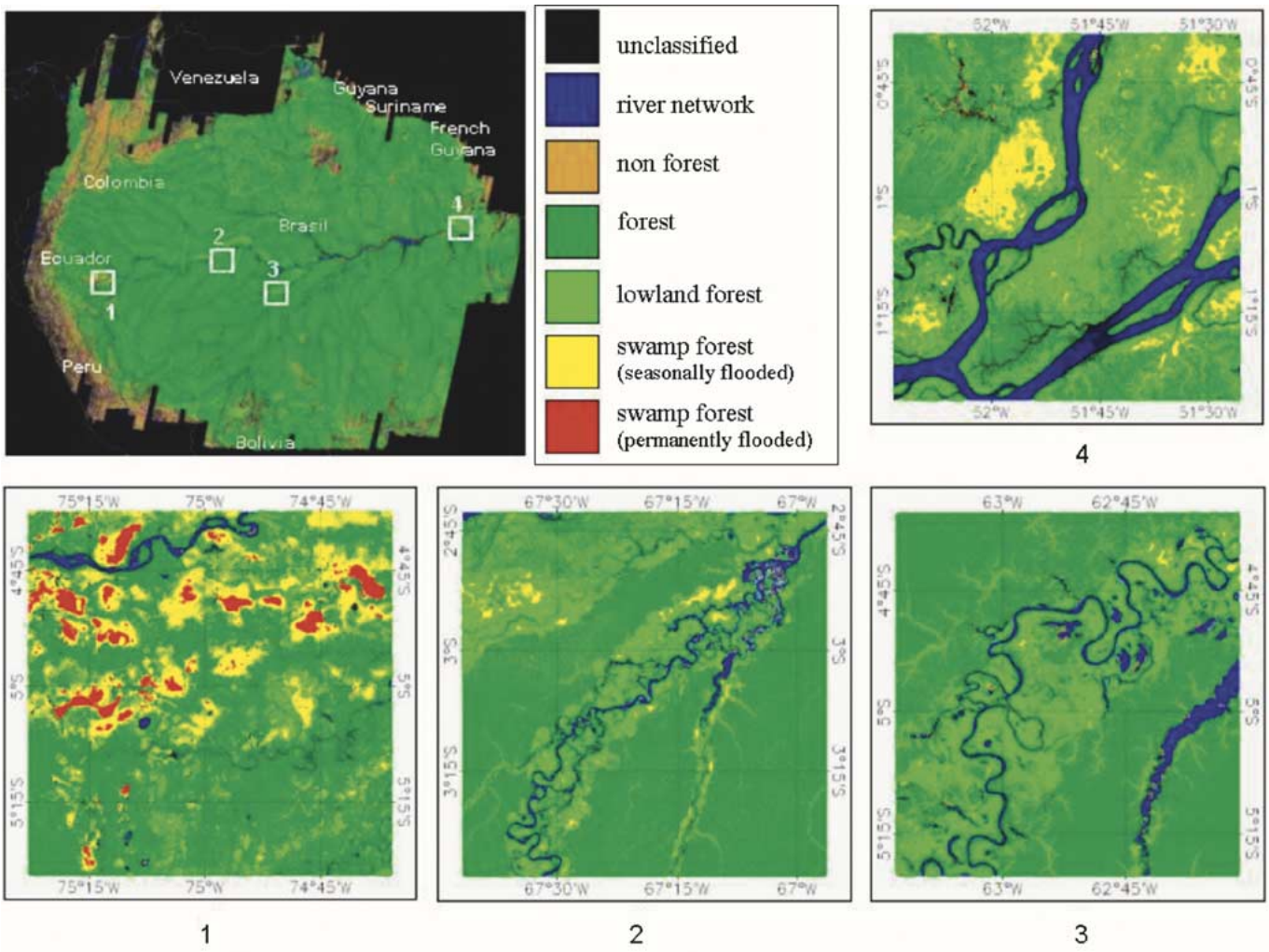

Fig. 10. Swamp forest map of the Amazon Basin compiled using the two-season GRFM radar mosaics and the ENMP classifier.

Based on these encouraging results, ENMP is applied to the entire two-season GRFM South America mosaic for a different thematic goal: the generation of a regional-scale map of the swamp forest extent in the Amazon Basin. Spaceborne radar data have been proven to be quite effective in mapping tropical swamp forests and their floodplains, which are environments of great interest for biodiversity and global change studies. Indeed, they harbor a series of important biochemical processes, such as nitrogen turnover and methane emission. Swamp forests can be discriminated from the surrounding lowland rain forest in radar imagery using simple texture measures. Texture is induced by the different canopy structure of the two forest types. Moreover, at L-band, radiation penetrates the vegetation layers, and therefore, also the flooding conditions can be monitored thanks to the double-bounce effect between the standing water and the trunks [74], [75].

Reference maps, delivered by the local forestry service (Instituto Nacional de Recursos Naturales INRENA) and generated by visual interpretation of Landsat TM imagery in combination with ground surveys, are employed to define classes of interest and locate training sites. The GRFM South America swamp forest map, compiled using the ENMP method, is shown in Fig. 10. In this figure, the insets reveal details of the radar map at full resolution (100 m) and bear evidence of the richness of thematic information and spatial details obtainable with this kind of ecosystemwide products. Inset 1 corresponds to an area located across the Maranon River in Peru that has been selected as one of the ENMP training sites. Insets 2, 3 (Central Amazon Basin—State of Amazonia), and 4 (State of Parà) correspond to testing sites employed for the map validation that was carried out by visual comparison with Landsat TM imagery.

Considered as a unique source of information on the extent and flooding conditions of the South America ecosystem [76], the ENMP swamp forest map is adopted as one information layer of a continental-scale land cover map of South America in the context of the Global Land Cover (GLC 2000) project [77].

IX. Summary and Conclusion

In this paper, a novel operational GRFM radar data-mapping approach, termed ENMP, suitable for processing radar datasets at the continental scale, is proposed. It consists of: 1) an application-dependent edge-preserving image smoothing stage and 2) a per-pixel two-stage hybrid learning classifier, whose core is a nearly optimal vector quantizer, called ELBG.

Due to difficulties in gathering reliable ground data in tropical forest areas at the regional scale, estimation of the abso-

lute accuracy of the GRFM thematic products is not realistic. Rather, the aim of this paper is to provide enough quantitative and qualitative evidence on the relative efficacy (in terms of mapping accuracy, computation time, and ease of use) of ENMP compared against alternative GRFM radar data-mapping systems. Collected qualitative and quantitative evidence show that ENMP: 1) in a forest/nonforest-mapping task provides a testing accuracy of 87%, which is in line with training accuracies, i.e., ENMP seems capable of generalizing over the entire dataset (as confirmed by a qualitative comparison of a radar map covering the entire Amazon Basin with a reference optical map at 1.2-km resolution); 2) is superior to two alternative approaches, INMP and SNMP, in terms of training accuracies; 3) is more robust than INMP and SNMP to changes in the geometric fragmentation of classes of interest; and 4) is competitive with INMP and SNMP in terms of processing time and largely superior to SNMP in terms of ease of use.

Results also show that, in line with theoretical expectations, the discrepancy between radar and reference optical maps increases when considering the boundary regions between *cerrado* (belonging to class NF) and humid forest ecosystems. A set of multitemporal radar images may be used to avoid such classification ambiguities. The foreseen JAXA Advanced Land Observing Satellite mission will possibly provide such multitemporal data.

Finally, ENMP is applied to the whole two-season GRFM South America mosaic to generate a map of the swamp forests and their flooding conditions at the regional scale. This map, in turn, provides a layer for a multisource global land cover map of South America generated in the context of the GLC 2000 project.

Based on these experiments, ENMP appears as a viable operational approach to the generation of regional-scale thematic maps using the GRFM radar mosaics.

ACKNOWLEDGMENT

The authors wish to thank NASDA/EORC, NASA/JPL, and ASF for access to the JERS-1 SAR mosaics. B. Chapman and P. Siqueira (JPL) are warmly thanked for their collaboration and help. The authors also wish to thank the anonymous referees for their valuable comments.

REFERENCES

[1] A. Rosenqvist, M. Shimada, B. Chapman, A. Freeman, G. F. De Grandi, S. Saatchi, and Y. Rauste, "The Global Rain Forest Mapping project—A review," *Int. J. Remote Sens.*, vol. 21, no. 6–7, pp. 1375–1387, Apr. 2000.

[2] P. Siqueira, S. Hensley, S. Shaffer, L. Hess, G. McGarragh, B. Chapman, and A. Freeman, "A continental scale mosaic of the Amazon Basin using JERS-1 SAR," *IEEE Trans. Geosci. Remote Sensing*, vol. 38, pp. 2638–2643, Nov. 2000.

[3] G. De Grandi, P. Mayaux, Y. Rauste, A. Rosenqvist, M. Simard, and S. Saatchi, "The Global Rain Forest Mapping project JERS-1 radar mosaic of tropical Africa: Development and product characterization aspects," *IEEE Trans. Geosci. Remote Sensing*, vol. 38, pp. 2218–2233, Sept. 2000.

[4] S. S. Saatchi, B. Nelson, E. Podest, and J. Holt, "Mapping land cover types in the Amazon basin using 1 km JERS-1 mosaic," *Int. J. Remote Sens.*, vol. 21, no. 6–7, pp. 1201–1234, Apr. 2000.

[5] M. Sgrenzaroli, H. Eva, and F. Achard, "Assessment of 100-m resolution L-band radar mosaics for regional forest change detection on lowland tropical forests of South America," in *Proc. IUFRO Conf. Remote Sensing and Forest Monitoring*, T. Zawila-Niedzwiecki and M. Brach, Eds., 2000, EUR 19530/EN, pp. 208–215.

[6] S. Sassan, G. F. De Grandi, and M. Simard, "Classification of JERS-1 image mosaic of Central Africa using a supervised multi-scale classifier of texture features," in *Proc. IGARSS*, Hamburg, Germany.

[7] M. Simard, S. Saatchi, and G. F. De Grandi, "Classification of the Gabon SAR mosaic using a wavelet based rule classifier," in *Proc. IGARSS*, Hamburg, Germany.

[8] L. Dutra, P. F. Hernandez, M. E. Mazzocato, C. M. De Souza, and C. Oliver, "Land cover classification based on multi-date JERS-1 imagery as a basis for deforestation detection," in *Proc. IGARSS*, Hamburg, Germany.

[9] P. Mayaux, G. F. De Grandi, Y. Rauste, M. Simard, and S. Saatchi, "Regional scale vegetation maps derived from the combined L-band GRFM and C-band CAMP wide area radar mosaics of Central Africa," *Int. J. Remote Sens.*, vol. 23, no. 7, pp. 1261–1282, Apr. 2002.

[10] M. Sgrenzaroli, G. F. De Grandi, R. Achard, and H. Eva, "Tropical forest cover monitoring: Estimates and validation from the GRFM JERS-1 radar mosaics using a wavelet zooming technique," *Int. J. Remote Sens.*, vol. 23, no. 7, pp. 1329–1355, Apr. 2002.

[11] M. Simard, S. Saatchi, and G. F. De Grandi, "The use of decision tree and multiscale texture for classification of JERS-1 SAR data over tropical forest," *IEEE Trans. Geosci. Remote Sensing*, vol. 38, pp. 2310–2321, Sept. 2000.

[12] M. Sgrenzaroli, A. Baraldi, G. F. De Grandi, F. Achard, and H. Eva, "High-resolution tropical forest mapping of the Amazon basin: A novel classification approach for the GRFM radar mosaic," in *Proc. IGARSS*, Sidney, Australia.

[13] G. Patane' and M. Russo, "The enhanced-LBG algorithm," *Neural Networks*, vol. 14, no. 9, pp. 1219–1237, Nov. 2001.

[14] ——, "ELBG implementation," *Int. J. Knowl. Based Intell. Eng. Syst.*, vol. 4, pp. 94–109, 2000.

[15] ——, "Fully automatic clustering system," *IEEE Trans. Neural Networks*, vol. 13, pp. 1285–1298, Nov. 2002.

[16] R. O. Duda, P. E. Hart, and D. G. Stork, *Pattern Classification*, 2nd ed. New York: Wiley, 2001.

[17] A. K. Jain and R. C. Dubes, *Algorithms for Clustering Data*. Englewood Cliffs, NJ: Prentice-Hall, 1988.

[18] A. Baraldi, P. Blonda, F. Parmiggiani, and G. Satalino, "Contextual clustering for image segmentation," *Opt. Eng.*, vol. 39, no. 4, pp. 1–17, Apr. 2000.

[19] A. Baraldi, M. Sgrenzaroli, and P. Smits, "Contextual clustering with label backtracking in remotely sensed image applications," in *Geospatial Pattern Recognition*, E. Binaghi, P. Brivio, and S. Serpico, Eds. Kerala, India: Research Signpost/Transworld Research, Apr. 2002, pp. 117–145.

[20] Y. Hashimoto and K. Tsuchiya, "Investigation of tropical rain forest in Central Amazonia, Brazil, based on JERS-1 SAR images," *J. Geography*, vol. 104, no. 6, pp. 827–842, 1995.

[21] D. Skole and C. J. Tucker, "Evidence for tropical deforestation, fragmented habitat, and adversely affected habitat in the Brazilian Amazon: 1978–1988," *Science*, vol. 260, pp. 1905–1910, 1993.

[22] A. Freeman, C. Krame, D. S. Alves, and B. Chapman, Tropical rain forest classification using JERS-1 SAR data, 1995.

[23] M. Schmidt, M. Keil, D. R. Scales, J. R. Dos Santos, and H. Kux, "Investigation of deforestation dynamics and land use changes by ERS-1 SAR data in Rondonia; Brazil," in *Proc. Int. Seminar Use and Applications ERS in Latin America*, Vina do Mar, Chile, Nov. 1996.

[24] L. V. Dutra, F. P. Hernandez, M. E. Mazzocato, R. C. De Souza, and M. Oliver, "Land cover classification based on multi-date JERS-1 imagery as a basis for deforestation detection," in *Proc. IGARSS*, vol. V.

[25] J. P. Malingreau and G. Duchossois, "The TREES ERS-1 SAR '94 project—Executive summary," in *Proc. Final Workshop ERS-1 Study*, 1994.

[26] D. H. Hoekman, "Synthesis for Latin American sites," in *Proc. Final Workshop ERS-1 Study*, 1994.

[27] M. Keil, D. R. Scales, D. Semmt, W. Winter, H. Honsch, and G. Lohmann, "Tropical rainforest investigation with ERS-1 SAR data in the region of Sena Maudureira, Acre/Brazil," in *Proc. Final Workshop ERS-1 Study*, 1994.

[28] J. Conway, "TREES ERS-1 Study 94 Workshop Final Report," in *Proc. Final Workshop ERS-1 Study*, 1994.

[29] C. Corves, R. Caves, R. Quegan, G. F. De Grandi, and E. Nezry, "Evaluating multi temporal ERS-1 SAR data for mapping forests and detecting forest clearing in the Manaus region of Brazil," in *Proc. Final Workshop ERS-1 Study*, 1994.

[30] M. G. Wooding and A. J. Batts, "Assessment of ERS-1 SAR data for monitoring deforestation Rondonia, Brazil," in *Proc. Final Workshop ERS-1 Study*, 1994.

[31] K. D. Grover, R. Quegan, L. V. Dutra, L. V. Yanasse, C. C. F. Hernandez, F. Sant'Anna, and A. Luckman, "ERS-1 observations and potential for use in tropical monitoring," in *Proc. Final Workshop ERS-1 Study*, 1994.
[32] D. H. Hoekman, "ERS-1 observations of tropical rain forest in Araracuara, Colombia," in *Proc. Final Workshop ERS-1 Study*, 1994.
[33] J. J. Van der Sanden, "Analysis of ERS-1 SAR data for Mabura Hill, Guyana," in *Proc. Final Workshop ERS-1 Study*, 1994.
[34] W. Bijker and D. H. Hoekman, "Monitoring of tropical rain forest and pastures with ERS-1," in *Proc. Final Workshop ERS-1 Study*, 1994.
[35] M. C. Dobson, "Land cover classification of tropical rain forests using orbital SAR and impacts of the natural and anthropogenic disturbance in species," EORC-NASDA, Tokyo, Japan, JERS-1 Sci. Prog. '99 IP Rep., Mar. 1999.
[36] L. V. Dutra, J. R. dos Santos, C. da Costa Freitas, E. M. de Leao Novo, D. S. Alves, P. H. Filho, D. C. Rennò, S. J. S. Sant'Anna, M. P. de Farias Costa, C. M. Ribeiro, S. M. Soares, and M. S. P. Lacruz, "The use of JERS-1 data for environment monitoring and resources assessment in Amazonia," EORC-NASDA, Tokyo, Japan, JERS-1 Sci. Prog. '99 IP Rep., Mar. 1999.
[37] E. Podest and S. Saatchi, "Application of multiscale texture in classifying JERS-1 radar data over tropical vegetation," *Int. J. Remote Sens.*, vol. 23, no. 7, 2002.
[38] J. C. Bezdek, T. R. Reichherzer, G. S. Lim, and Y. Attikiouzel, "Multiple-prototype classifier design," *IEEE Trans. Syst. Man, Cybern.—Appl. Rev.*, vol. 28, pp. 67–79, Feb. 1998.
[39] C. Johnston, *Geographic Information Systems in Ecology*. Oxford, U.K.: Blackwell Science, 1998.
[40] J. A. Richards, *Remote Sensing Digital Image Analysis*. Berlin, Germany: Springer-Verlag, 1986.
[41] M. R. Spiegel, *Statistics*. New York: McGraw-Hill, 1961.
[42] C. Bishop, *Neural Networks for Pattern Recognition*. Oxford, U.K.: Oxford Univ. Press, 1995.
[43] J. P. Malingreau, F. Achard, G. D'Souza, H. J. Stibig, J. D'Souza, C. Estreguil, and H. Eva, "AVHRR for global tropical forest monitoring: The lessons of the TREES project," *Remote Sens. Rev.*, vol. 12, pp. 29–40, 1995.
[44] TRFIC Tropical Rain Forest Information Center. NASA's Earth Science Information Partnership. [Online]. Available: http://bsrsi.msu.edu/trfic/index.html.
[45] FAO, "Global forest resources assessment 2000 (FRA 2000)," Food Agricult. Org. United Nations, Rome, Italy, No. 140, 2002.
[46] F. Achard, H. D. Eva, H.-J. Stibig, P. Mayaux, F. Galego, T. Richards, and J. P. Malingreau, "Determination of deforestation rates of the world's humid tropical forests," *Science*, vol. 297, pp. 999–1002, 2002.
[47] G. De Grandi, P. Mayaux, M. Massart, A. Baraldi, and M. Sgrenzaroli, "A vegetation map of the central Congo basin derived from microwave and optical remote sensing data using variable resolution classification approach," in *Proc. IGARSS*, Sidney, Australia.
[48] M. Simard, G. De Grandi, and K. Thomson, "Adaptation of the wavelet transform for the construction of multiscale texture maps of SAR images," *Can. J. Remote Sens.*, vol. 24, no. 3, pp. 264–285, 1998.
[49] M. Simard, G. F. De Grandi, K. P. B. Thomson, and G. B. Benie', "Analysis of speckle noise contribution on wavelet decomposition of SAR images," *IEEE Trans. Geosci. Remote Sensing*, vol. 36, pp. 1953–1962, Nov. 1998.
[50] S. Fukuda and H. Hirosawa, "A wavelet-based texture feature set applied to classification of multifrequency polarimetric SAR images," *IEEE Trans. Geosci. Remote Sensing*, vol. 37, pp. 2282–2286, Sept. 1999.
[51] ——, "Suppression of speckle in synthetic aperture radar images using wavelets," *Int. J. Remote Sens.*, vol. 19, pp. 507–519, 1998.
[52] ——, "Smoothing effect of wavelet-based speckle filtering: The Haar basis case," *IEEE Trans. Geosci. Remote Sensing*, vol. 37, p. 1164, Mar. 1999.
[53] A. Niedermeier, E. Romaneeßen, and S. Lehner, "Detection of coastlines in SAR images using wavelet methods," *IEEE Trans. Geosci. Remote Sensing*, vol. 38, pp. 2270–2281, Sept. 2000.
[54] A. Ferretti, C. Prati, and F. Rocca, "Multibaseline InSAR DEM construction: The wavelet approach," *IEEE Trans. Geosci. Remote Sensing*, vol. 37, pp. 705–715, Mar. 1999.
[55] F. De Grandi, J. S. Lee, D. Schuler, G. Kattemborg, F. Holecz, P. Pasquali, and M. Simard, "Singularity analysis with wavelets in polarimetric SAR imagery for vegetation mapping applications," in *Proc. IGARSS*, Hamburg, Germany.
[56] F. De Grandi, J. S. Lee, M. Simard, and H. Wakabayashi, "Speckle filtering, segmentation and classification of polarimetric SAR data: A unified approach based on the wavelet transform," in *Proc. IGARSS*, Honolulu, HI, 2000.
[57] F. De Grandi, J. S. Lee, P. Siqueira, A. Baraldi, and M. Simard, "Segmentation and labeling of polarimetric SAR data: Can wavelets help?," in *Proc. IGARSS*, Sydney, Australia, 2001.
[58] S. Mallat, *A Wavelet Tour of Signal Processing*, 2nd ed. San Diego, CA: Academic, 1999, pp. 163–219.
[59] S. Mallat and S. Zhong, "Characterization of signals from multiscale edges," *IEEE Trans. Pattern Anal. Machine Intell.*, vol. 14, pp. 710–732, July 1992.
[60] S. Mallat and W. Hwang, "Singularity detection and processing with wavelets," *IEEE Trans. Inform. Theory*, vol. 38, pp. 617–642, Mar. 1992.
[61] Q. Jackson and D. Landgrebe, "An adaptive classifier design for high-dimensional data analysis with a limited training data set," *IEEE Trans. Geosci. Remote Sensing*, vol. 39, pp. 2664–2679, Dec. 2001.
[62] R. Kohavi, "A study of cross-validation and bootstrap for accuracy estimation and model selection," in *Proc. Int. Joint Conf. Artificial Intelligence*, Montreal, QC, Canada, 1995.
[63] RSI, *ENVI User's Guide*. Vienna, VA: Research Systems, Inc., 2002.
[64] E. Backer and A. K. Jain, "A clustering performance measure based on fuzzy set decomposition," *IEEE Trans. Pattern Anal. Machine Intell.*, vol. PAMI-3, pp. 66–75, Jan. 1981.
[65] G. M. Foody, "Status of land cover classification accuracy assessment," *Remote Sens. Environ.*, vol. 80, pp. 185–201, 2002.
[66] M. Beauchemin and K. Thomson, "The evaluation of segmentation results and the overlapping area matrix," *Int. J. Remote Sens.*, vol. 18, no. 18, pp. 3895–3899, 1997.
[67] P. A. Furley, J. Proctor, and J. Ratter, *Nature and Dynamics of the Forest-Savanna Boundaries*. London, U.K.: Chapman & Hall, 1992.
[68] K. Landis, "The measurement of observer agreement for categorical data," *Biometrics*, vol. 33, pp. 159–174, 1977.
[69] R. Congalton and K. Green, *Assessing the Accuracy of Remotely Sensed Data: Principles and Practices*. Boca Raton, FL: Lewis, 1999.
[70] P. H. Swain and S. M. Davis, *Remote Sensing: The Quantitative Approach*. New York: McGraw-Hill, 1978.
[71] J. Carletta, "Assessing agreement on classification tasks: The Kappa statistic," *Comput. Linguist.*, vol. 22, no. 2, pp. 249–254, 1996.
[72] P. Peralta and P. Mather, "An analysis of deforestation patterns in the extractive reserves of Acre, Amazonia, from satellite imagery: A landscape ecological approach," *Int. J. Remote Sens.*, vol. 21, no. 13–14, pp. 2555–2570, 2000.
[73] Landscape Ecology Lab. Landscape ecology syllabus. Duke Univ., Landscape Ecology Lab.. [Online]. Available: http://www.env.duke.edu/lel/env214/le_syl.html.
[74] P. Mayaux, G. F. De Grandi, Y. Rauste, M. Simard, and S. Saatchi, "Regional scale vegetation maps derived from the combined L-band GRFM and C-band CAMP wide area radar mosaics of Central Africa," *Int. J. Remote Sens.*, vol. 23, no. 7, pp. 1261–1282, Apr. 2002.
[75] G. F. De Grandi, P. Mayaux, J. P. Malingreau, A. Rosenqvist, S. Saatchi, and M. Simard, "New perspectives on global ecosystems from wide-area radar mosaics: Flooded forest mapping in the tropics," *Int. J. Remote Sens.*, vol. 21, no. 6–7, pp. 1235–1250, Apr. 2000.
[76] H. D. Eva, E. E. de Miranda, C. M. Di Bella, V. Gond, O. Huber, M. Sgrenzaroli, S. Jones, A. Countinho, A. Dorado, M. Guimaraes, C. Elvidge, F. Achard, A. S. Belward, E. Batholome', A. Baraldi, G. De Grandi, P. Vogt, S. Fritz, and A. Hartley, "A vegetation map of South America," Eur. Commiss., Brussels, Belgium, Rep. EUR 20159 EN, 2002.
[77] E. Bartholomé and A. S. Belward, "GLC2000: A new approach to global land cover mapping from Earth Observation data," *Int. J. Remote Sens.*, to be published.

Matteo Sgrenzaroli received the laurea degree in environmental engineering from Politecnico Milano, Milan, Italy, in 1997, and the Ph.D. degree from Wageningen Agricultural University, Wageningen, The Netherlands, in 2004.

In 1997, he was a student team member at the Space Application Institute, European Commission Joint Research Centre (JRC) and carried out analyses of multitemporal ERS-1 and JERS-1 SAR data for rice paddies monitoring (Southeast Asia Radar Rice Investigation project). In 1998, he was instrumental in organizing and took part in the Changri Nup glacier monitoring expedition promoted by University of Brescia, within the context of the EV-K2 project of National Research Council of Italy. He was a grant holder at JRC from 1999 to 2001, working on tropical deforestation monitoring using continental-scale JERS-1 radar mosaics. From October 2001 to February 2003, he was Project Manager at 3DVeritas, a spinoff company funded by the EC-JRC. Here, he supervised the development of a 3-D surface modeling software toolbox employing laser scanner data and digital images as input data. In 2003, he joined TOPOTEK, Brescia, Italy, a center of competence in surveying and geomatics connected to the University of Brescia.

Andrea Baraldi received the laurea degree in electronic engineering from the University of Bologna, Bologna, Italy, in 1989. His master thesis focused on the development of unsupervised clustering algorithms for optical satellite imagery.

He is currently a Research Associate with ISAC-CNR, National Research Council (CNR), Bologna, Italy. From 1989 to 1990, he was a Research Ssociate at CIOC-CNR, an Institute of the National Research Council, Bologna, and served in the army at the Istituto Geografico Militare in Florence, working on satellite image classifiers and GIS. As a consultant at ESA-ESRIN, Frascati, Italy, he worked on object-oriented applications for GIS from 1991 to 1993. From December 1997 to June 1999, he joined the International Computer Science Institute, Berkeley, CA, with a postdoctoral fellowship in artificial intelligence. Since his master thesis, he has continued his collaboration with ISAO-CNR, Bologna. He was a Post-Doc Researcher with the European Commission Joint Research Center, Ispra, Italy, where he worked on the development and validation of algorithms for the automatic thematic information extraction from wide-area radar maps of forest ecosystems. His main interests center on image segmentation and classification, with special emphasis on texture analysis and neural network applications employing contextual image information.

Dr Baraldi is an Associate Editor of IEEE TRANSACTIONS ON NEURAL NETWORKS.

Gianfranco D. De Grandi (M'90–SM'96–F'02) received the doctorate degree in physics engineering (with honors) from the Politecnico di Milano, Milan, Italy, in 1973.

Since 1977, he has been with the European Commission Joint Research Center (JRC), Ispra, Italy, where he has performed research in signal processing for application areas such as gamma ray spectroscopy, data communications, and radar remote sensing. In 1985, he was a Visiting Scientist at Bell Communications Research, Morristown, NJ, where he participated in the design of METROCORE, one of the first research projects for gigabit rate metropolitan area networks. From 1997 to 2001, he was an Assistant Professor with the Faculté de Feresterie et Geomatique, Université Laval, Laval, QC, Canada. His current research interests include global-scale forest mapping using high-resolution spaceborne SAR, wavelet multiresolution techniques for the approximation and analysis of SAR imagery, topography sensing using polarimetric SAR data, and the statistics of polarimetric synthesized SAR images. He is Principal Investigator of the Japan Aerospace Exploration Agency (JAXA), Tokyo, Japan, Global Rain Forest Mapping and Global Boreal Forest Mapping projects, the JAXA ALOS research program, and the European Space Agency ESA EO Exploitations projects.

Dr. De Grandi was elected IEEE Fellow, with the citation "For contributions to continental-scale vegetation mapping using high-resolution SAR mosaics, and in the area of information extraction from SAR data." He is a member of the IEEE Geoscience and Remote Sensing society, the IEEE Signal Processing society, the Planetary Society, Pasadena CA, and the Society of Industrial and Applied Mathematics.

Hugh Eva is a Research Officer with the European Commission's Joint Research Centre, Ispra, Italy. He specializes in the use of remotely sensed data for mapping fires and forests in tropical ecosystems. He was recently responsible for producing the South American map of the Global Land Cover 2000 project from SPOT VEGETATION data. Before this, he was the Latin America coordinator of the TREES (the Tropical Ecosystem Environment observation by Satellite) project, which was set up to monitor and measure changes in the tropical forest belt, using remote sensing techniques.

Frédéric Achard received the master's degree from the Ecole Polytechnique, Paris, France in 1984, the master's degree from the Ecole Nationale du Génie Rural, des Eaux et des Forêts, Paris, in 1986, and the Ph.D. degree in tropical ecology and remote sensing (with honors) from Toulouse University, Toulouse, France, in 1989.

From 1986 to 1990, he has been with the Institute for the International Vegetation Map (CNRS/University), Toulouse, France, where he performed research in optical remote sensing techniques for monitoring vegetation dynamics in West Africa. In 1990 and 1991, he was detached national expert from the French Ministry of Agriculture and Forest working at the Joint Research Centre, Ispra, Italy, where he started a research activity over Southeast Asia in the framework of the Tropical Ecosystem Environment observations by Satellite (TREES) project. In 1992, he joined the European Commission Joint Research Centre to conduct the first phase of TREES project. From 1996 to 2001, he led the second phase of the TREES project in the Global Vegetation Monitoring unit now part of the JRC Institute for Environment and Sustainability and initiated in 1999 activities of forest cover monitoring in Siberia. His current research interests include development of earth observation techniques for tropical and boreal forest regional assessments and for global tropical forest monitoring.